Since January 2020 Elsevier has created a COVID-19 resource centre with free information in English and Mandarin on the novel coronavirus COVID-19. The COVID-19 resource centre is hosted on Elsevier Connect, the company's public news and information website.

THE JOURNAL OF BIOLOGICAL CHEMISTRY VOL. 281, NO. 45, pp. 34610–34616, November 10, 2006

Structural Basis of Neutralization by a Human Anti-severe Acute Respiratory Syndrome Spike Protein Antibody, 80R*[S]

Received for publication, April 6, 2006, and in revised form, July 19, 2006 Published, JBC Papers in Press, September 5, 2006, DOI 10.1074/jbc.M603275200

William C. Hwang[‡1], Yaqiong Lin[‡1], Eugenio Santelli[‡], Jianhua Sui[§], Lukasz Jaroszewski[‡], Boguslaw Stec[‡], Michael Farzan[¶], Wayne A. Marasco[§], and Robert C. Liddington[‡2]

From the [‡]Infectious and Inflammatory Disease Center, Burnham Institute for Medical Research, La Jolla, California 92037, the [§]Department of Cancer Immunology and AIDS, Dana-Farber Cancer Institute, Boston, Massachusetts 02115, and the [¶]Department of Microbiology and Molecular Genetics, Harvard Medical School, New England Primate Research Center, Southborough, Massachusetts 01772

Severe acute respiratory syndrome (SARS) is a newly emerged infectious disease that caused pandemic spread in 2003. The etiological agent of SARS is a novel coronavirus (SARS-CoV). The coronaviral surface spike protein S is a type I transmembrane glycoprotein that mediates initial host binding via the cell surface receptor angiotensin-converting enzyme 2 (ACE2), as well as the subsequent membrane fusion events required for cell entry. Here we report the crystal structure of the S1 receptor binding domain (RBD) in complex with a neutralizing antibody, 80R, at 2.3 Å resolution, as well as the structure of the uncomplexed S1 RBD at 2.2 Å resolution. We show that the 80R-binding epitope on the S1 RBD overlaps very closely with the ACE2-binding site, providing a rationale for the strong binding and broad neutralizing ability of the antibody. We provide a structural basis for the differential effects of certain mutations in the spike protein on 80R *versus* ACE2 binding, including escape mutants, which should facilitate the design of immunotherapeutics to treat a future SARS outbreak. We further show that the RBD of S1 forms dimers via an extensive interface that is disrupted in receptor- and antibody-bound crystal structures, and we propose a role for the dimer in virus stability and infectivity.

Severe acute respiratory syndrome (SARS),[3] a newly emerged infectious disease, claimed 813 lives from ~8000 patients during a 2003 global epidemic. In severe illness, influenza-like symptoms quickly progress to pneumonia, hypoxia, and acute respiratory distress and failure, resulting in 10% overall death rate with exceptionally high mortality among the elderly (1). A novel coronavirus (SARS-CoV) has been identified as the etiological agent of SARS. The SARS-CoV surface spike protein S mediates viral entry into the host cell (2) and includes two functional domains as follows: S1 (Gly^{13}–Arg^{667}) and S2 (Ser^{668}–Thr^{1255}). S1 contains the host-specific receptor binding domain (RBD), whereas S2 mediates fusion between viral and host cell membranes (3). Angiotensin-converting enzyme 2 (ACE2) was identified as a functional receptor for the SARS-CoV (4). The recently determined structure of the S1-RBD in complex with the extracellular domain of ACE2 (5) illustrates the structural basis for the initial step of virus-host recognition.

As the mediator of host-specific SARS infection and a major viral surface antigen, the S protein is an attractive candidate for both vaccine development and immunotherapy. Marasco and co-workers (6) previously identified a potent neutralizing human monoclonal antibody against the S1 RBD, designated "80R," from two nonimmune (*i.e.* not restricted by B cell recombination) human antibody libraries. 80R binds S1 with nanomolar affinity, blocks the binding of S1 to ACE2, prevents the formation of syncytia *in vitro* (6), and inhibits viral replication *in vivo* (7). Deletion studies have shown that the 80R epitope on S1 is located in the minimal ACE2 binding domain, between residues 324 and 503 (6, 7).

Here, we report the crystal structure of the S1-RBD both alone and in complex with 80R. The complex structure reveals the basis of the broad neutralizing ability of 80R and will facilitate the design of immunotherapeutics in the case of a future SARS outbreak. We further show that the S1-RBD forms dimers by means of an unexpected reorganization of the region distal to the receptor-binding surface. The dimers are disrupted by complex formation, and we discuss the possibility that receptor binding plays an active role in the initial steps of viral uncoating.

EXPERIMENTAL PROCEDURES

Protein Expression, Purification, and Crystallization—The gene encoding single chain (VH-linker-VL) antibody 80R (scFv) was cloned into pET22b (Novagen) containing an N-terminal periplasmic secretion signal pelB, and a thrombin-removable C-terminal His_6 tag. 80R was overexpressed in BL21(DE3) cells at 30 °C for 15 h with 1 mM isopropyl 1-thio-β-D-galactopyranoside. Protein was purified by HisBind nickel-nitrilotriacetic acid (Novagen) column and Superdex 200 gel

* This work was supported by National Institutes of Health Grants DAMD17-03-2-0038 (to R. C. L.), AI28785, AI48436, AI061318, and AI053822 (to W. A. M.). The costs of publication of this article were defrayed in part by the payment of page charges. This article must therefore be hereby marked "*advertisement*" in accordance with 18 U.S.C. Section 1734 solely to indicate this fact.

The atomic coordinates and structure factors (code 2GHV and 2GHW) have been deposited in the Protein Data Bank, Research Collaboratory for Structural Bioinformatics, Rutgers University, New Brunswick, NJ (http://www.rcsb.org/).

[S] The on-line version of this article (available at http://www.jbc.org) contains Fig. S1.

[1] Both authors contributed equally to this work.

[2] To whom correspondence should be addressed: Burnham Institute for Medical Research, 10901 North Torrey Pines Rd., La Jolla, CA 92037. Tel.: 858-646-3136; Fax: 858-792-1768; E-mail: rlidding@burnham.org.

[3] The abbreviations used are: SARS, severe acute respiratory syndrome; CoV, coronavirus; ACE2, angiotensin-converting enzyme 2; RBD, receptor-binding domain; CDR, complementarity-determining region.

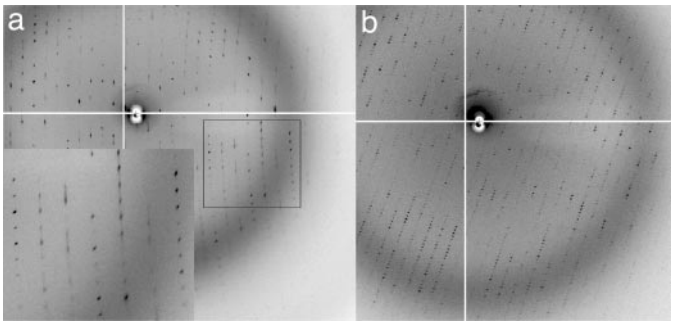

FIGURE 1. **Diffraction patterns of complex crystal.** The complex crystals display a lattice-translocation defect caused by translocations in the crystal packing between neighboring layers along the *a** direction. *a*, *a** is nearly vertical, in the plane of the paper, and the defect results in periodic sharp-diffuse-diffuse rows of diffraction intensities (the *bottom left quadrant* is a zoom-in of the *boxed area*). *b*, *a** is nearly parallel to the x-ray beam and perpendicular to the paper, and the defect is not evident.

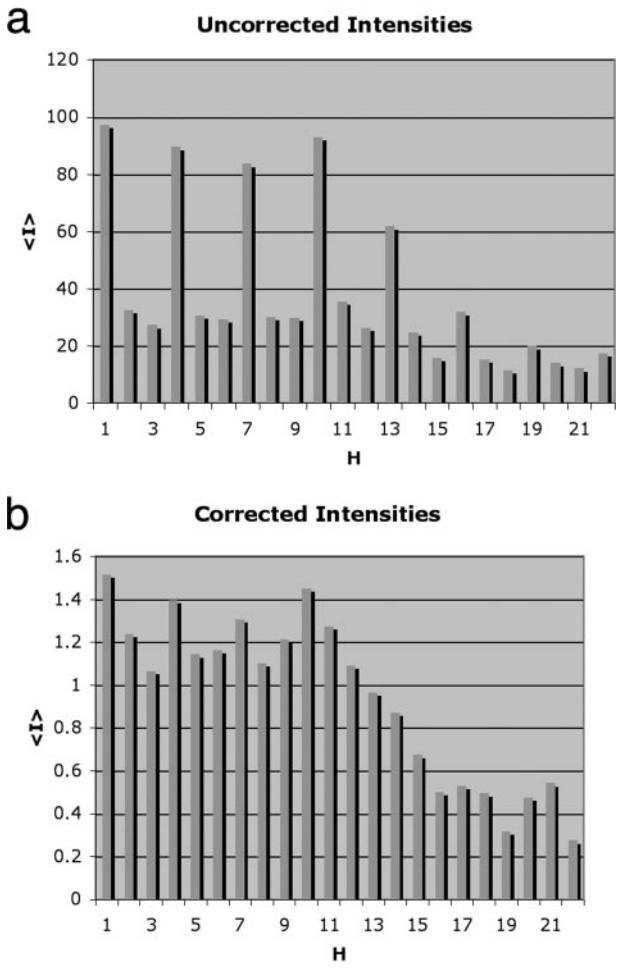

FIGURE 2. ***h* layer intensities before and after correction.** *a,* the lattice defect results in a strong-weak-weak pattern of intensities along *h*, which were corrected (*b*) according to the procedure of Wang *et al.* (10).

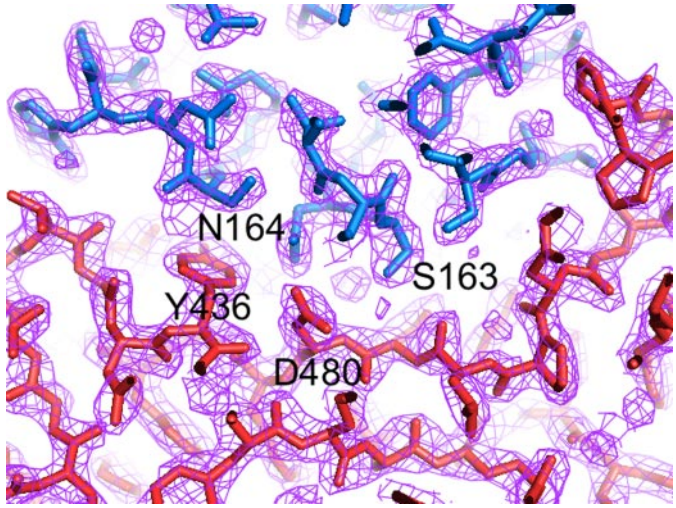

FIGURE 3. **Stereo $2F_o - F_c$ electron density map of the S1-RBD-80R complex at the S1-80R interface.** S1 and 80R residues are shown in *red* and *blue*, respectively, with selected residues labeled. Contour level = 1.5σ.

filtration chromatography (Amersham Biosciences) after thrombin digestion.

The gene encoding S1-RBD (residues 318–510) was cloned into vector pAcGP67A (Pharmingen) containing an N-terminal gp67 secretion signal and a thrombin-cleavable C-terminal His_6 tag. It was expressed in Sf9 cells (Invitrogen) with a multiplicity of infection = 5 for 72 h. Similar to 80R, S1-RBD was purified from the media with HisBind nickel-nitrilotriacetic acid and Superdex 200 columns, with thrombin digestion. *N*-Linked glycosylation was removed by incubation with peptide:*N*-glycosidase F (New England Biolabs) at 23 °C, as monitored by SDS-PAGE. S1 RBD-80R complexes were formed by mixing the two purified components and isolated by gel filtration with Superdex 200 in 10 mM Tris-HCl, 150 mM NaCl, pH 7.4. Peak fractions were pooled and concentrated to ~7 mg/ml. For S1-RBD crystal growth, the protein was also concentrated to ~7 mg/ml.

Crystals grew by the hanging drop vapor diffusion method at 17 °C over ~21 days. For S1-RBD, 2 μl of S1-RBD was mixed with an equal volume of well solution containing 4% w/v polyethylene glycol 4000, 0.1 M sodium acetate, pH 4.6. For the S1-RBD-80R complex, 2 μl of the complex was mixed with an equal volume of well solution containing 12.5% w/v polyethylene glycol 4000, 0.1 M sodium acetate, 0.2 M ammonium sulfate, pH 4.6.

Data Collection, Structure Determination, and Refinement—X-ray diffraction data were collected at the National Synchrotron Light Source beamline X6A and X29A for S1-RBD crystals, the Stanford Synchrotron Radiation Laboratory beamline 11.1, and at the Advanced Light Source beamlines 5.0.3 and 12.3.1 for crystals of the S1-RBD-80R complex. Glycerol (25%) was used as a cryoprotectant in both cases. All the data were processed with DENZO and SCALEPACK or with the HKL2000 package (8). Crystals of S1 RBD adopt space group $P4_32_12$ with unit cell dimensions $a = 75.9$ and $c = 235.8$ (Table 1).

Crystals of the S1-RBD-80R complex adopt space group $P2_1$ with unit cell dimensions $a = 47.5$, $b = 175.9$, $c = 67.6$, $\beta = 96.6°$. The crystals display a lattice-translocation defect in which a fraction of the layers have a translational offset, resulting in periodic sharp and diffuse rows of reflections (Fig. 1). Similar defects were first described by Bragg and Howells (9). Different crystals displayed different degrees of lattice defects, and data merged poorly between crystals. By using a single crystal we were able to collect a data set of good quality with a final $R_{MERGE} = 0.145$ and completeness of 93.8% to 2.3 Å resolution. Processing the data required careful optimization of integra-

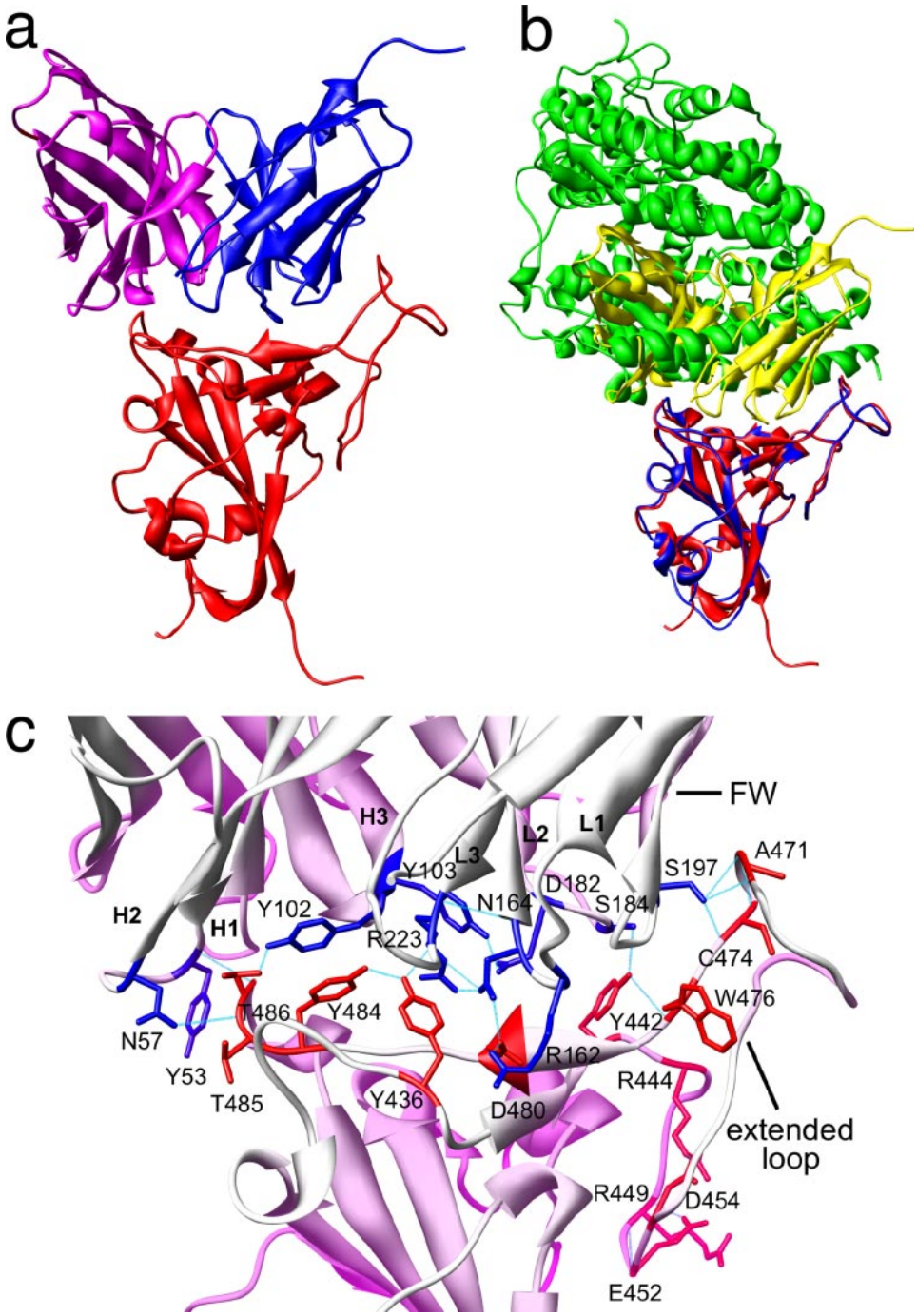

FIGURE 4. **Structure of the S1-RBD-80R complex.** *a*, overall structure of the complex. Antibody variable region light chain is in *blue*, and heavy chain is in *magenta*; S1-RBD is in *red*. *b*, comparison between the S1 RBD-80R complex (*red* and *yellow)* and the S1 RBD-ACE2 complex (*blue* and *green*) overlaid on the S1-RBD domain. *c*, close-up of the interface. Selected S1 side chains are in *red*; 80R is in *blue*; hydrogen bonds are in *cyan*. CDRs (*L1–L3* and *H1–H3*) and the framework (*FW*) loop (interacting with the extended loop of S1) are labeled. There is an aromatic ring stacking between Tyr^{484} (S1) and Tyr^{102} (80R). Tyr^{484} and Tyr^{102} are in turn coordinated by hydrogen bonds between Tyr^{486} (S1) and Tyr^{102} (80R) and Tyr^{53} (80R), and Tyr^{484} (S1) and Tyr^{436} (S1), respectively. Another intermolecular hydrogen bond occurs between Leu^{478} (S1) and Ser^{163} (80R). Asn^{164} (80R) makes intramolecular hydrogen bonds with Arg^{223} (80R). Intramolecular hydrogen bonding between Tyr^{103} (80R) and Asp^{182} (80R) may be important for maintaining the 80R structure at the interface and may be important for S1 RBD-80R binding. Cys^{474} (S1), Ala^{471} (S1), and Ser^{197} (80R) form another intermolecular hydrogen bonds that may stabilize the S1 RBD-80R interface.

tion profiles and the imposition of a fixed mosaicity (0.45°). Correlation between the offset layers caused the appearance of a strong off-origin peak (65% of the origin) in the native Patterson map at (1/3, 0, 0), indicating that the dislocation occurred along the a^* direction. Additional features of the Patterson map were visible at ~1/10 of the origin peak and provided a measure of the severity of the defect among different crystals. The averaged intensity for the layers of reflections showed a periodic variation that corresponded to the sharp and diffuse layers, and we used the procedure developed by Wang *et al.* (10) to correct for the intensity modulation (Fig. 2). We calculated average intensities for individual h layers, and applied a correction to the intensities using Equation 1,

$$I_{COR} = I_{MEAS}/(A + B\cos(2\pi h\Delta x)) \quad \text{(Eq. 1)}$$

where A and B were obtained by least square fitting of the averaged measured intensities. The ratio of the parameters B and A (B/A = 0.65) coincided with the height ratio of the Patterson peak at (1/3, 0, 0), as required by the lattice-translocation theory presented by Wang. The corrected intensity distribution (Fig. 2*b*) was used for the structure solution and the refinement.

The structure of the S1-RBD-80R complex was determined using the Joint Center for Structural Genomics molecular replacement pipeline (11), which employs a modified version of MOLREP (12), and independently using PHASER (13), with the S1-RBD domain from the S1-RBD-ACE2 complex and the scFv domain from the scFv-turkey egg-white lysozyme complex (Protein Data Bank code 1DZB) as search models. The asymmetric unit contains two molecules of S1 RBD-80R. The final model includes residues 318–505 (molecule 1) and 319–509 (molecule 2) of S1 RBD and residues 1–245 (molecule 1) and 1–244 (molecule 2) of 80R, and 470 water molecules. No electron density was observed for the artificial poly(Gly/Ser) inter-domain linker. Initial solutions from molecular replacement were subjected to several rounds of refinement with the program REFMAC5 (14) with simulated annealing in CNS (15) and manual model rebuilding with programs O (16) and Coot (17).

The structure of uncomplexed S1-RBD (which showed no lattice defects) was determined by molecular replacement with PHASER (13) using S1-RBD from the structure of the S1-RBD-ACE2 complex (Protein Data Bank code 2AJF) as the search model. The asymmetric unit contains two molecules of S1-RBD arranged as a symmetric dimer. The final model includes residues 320–503 of both monomers and 152 water molecules.

Geometric parameters are excellent as assessed with PROCHECK (18) (Table 1). Final R_{WORK}/R_{FREE} values are 18.2/21.3 and 24.8/29.5 for the uncomplexed S1-RBD and the S1-RBD-80R complex, respectively. The higher R values for the S1 RBD-80R complex can likely be explained by the limitations of the lattice defect model and the integration of weak, elongated spots, as discussed previously (10). Notwithstanding, the final electron density map for the S1 RBD-80R complex is of excellent quality (Fig. 3), and the model-to-map correlation is above 0.9 for most of the residues at 2.3 Å resolution. Coordinates have been deposited in the Protein Data Bank with codes 2GHV (S1-RBD) and 2GHW (S1-RBD-80R complex).

TABLE 1
Data collection and refinement statistics

	S1-RBD	S1-RBD-80R
Data collection		
Cell parameters	$a = 75.9$, $c = 235.9$ Å	$a = 47.5$, $b = 175.9$, $c = 67.6$ Å; $\beta = 96.6°$
Space group	$P4_32_12$	$P2_1$
Resolution (Å)	2.2	2.3
Total reflections	233011	159047
Unique reflections	36036	51915
Completeness (%)[a]	99.9 (99.9)	93.8 (87.0)
Average $I/\sigma(I)$[a]	24.7 (2.0)	8.8 (1.9)
R_{merge}[a]	0.098 (0.739)	0.145 (0.571)
Redundancy	6.5	3.1
Refinement		
R_{work}[b]	0.182 (0.230)	0.248 (0.301)
R_{free} (5% data)[b]	0.213 (0.289)	0.295 (0.391)
r.m.s.d. bond distance (Å)[c]	0.013	0.009
r.m.s.d. bond angle (°)	1.49	1.22
Average B value	50.0	37.1
Solvent atoms	152	470
Ramachandran plot		
Residues in most favored regions	276	631
Residues in additional allowed regions	35	81
Residues in generously allowed regions	3	5
Residues in disallowed regions	0	0

[a] Numbers in parentheses correspond to the highest resolution shell (2.28–2.20 Å for S1 RBD; 2.29–2.38 Å for S1 RBD-80R).
[b] Numbers in parentheses correspond to the highest resolution shell (2.26–2.20 Å for S1 RBD; 2.29–2.38 Å for S1 RBD-80R).
[c] r.m.s.d., root meant square deviation.

RESULTS AND DISCUSSION

Structure of the S1-RBD-80R Complex—We determined the crystal structure of the S1-RBD-80R complex at 2.3 Å resolution (Figs. 3 and 4 and Table 1). The S1 RBD has a very similar structure to that in the ACE2 complex (Fig. 4*b*). The complex interface involves all six antibody complementarity-determining region (CDR) loops, which protrude into the concave surface on the S1 receptor-binding motif. Chothia *et al.* (19, 20) showed that there exists only a small repertoire of main chain conformations for 5 of the 6 CDR loops (excluding H3, which is often long and highly variable in structure) and that these structures can be predicted from their amino acid sequences. For the CDR loops of 80R, loops L2, L3, H1, and H2 adopt main chain conformations close to those predicted by Chothia. However, the L1 loop is atypical, although similar to that of the anti-human immunodeficiency virus-gp41 antibody (Protein Data Bank code 1DFB). The H3 loop is short and well ordered. A loop that is classically considered part of the framework (between β-strands D and E) (Fig. 4*c* and Table 2) also plays a major role in the interface; the "extended loop" (5) of S1 wraps around this framework loop making multiple contacts.

Although ACE2 employs a different recognition mode (dominated by a helix that lines the concave surface of S1), the 80R epitope on S1 overlaps very closely with the ACE2-binding surface (Fig. 4*b*). Thus, of the 29 residues (between 426 and 492) on S1 that contact 80R, 17 of these also make interactions in the S1-ACE2 interface. The S1-80R interface buries ~2200 Å^2 of protein surface, compared with ~1700 Å^2 for S1-ACE2. The "gap volume," a measure of shape complementarity (21), is ~4000 Å^3 for the S1-80R interface, about half that of S1-ACE2 (~7000 Å^3). The larger buried surface and smaller gap volume provide a rationale for the stronger binding and neutralizing activity of the antibody.

TABLE 2
Contact residues between 80R and S1 RBD

80R residues are listed on the top line and grouped under CDR or framework region (FR). S1 residues in contact with 80R residues are listed in subsequent lines. S1-ACE2 and S1-80R interfaces share many common S1 residues, except for 5 residues (404, 443, 460, 462, and 463) which are found only at the S1-ACE2 interface, while 12 residues (433, 437, 439, 469, 470, 471, 474, 476, 478, 480, 485, and 492) are found only at the S1-80R interface.

CDR H1			CDR H2						CDR H3					FRL1	CDRL1		
S31	Y32	A33	V50	I51	S52	Y53	N57	Y59	D99	R100	S101	Y102	D105	R150	V161	R162	S163
T487	Y491	T486	T486	T486	T486	R426	R426	S432	T487	Y491	Y436	S432	Y491	L472	D480	Y436	L478
G488		T487				T485	T485	T485	Y491		G482	Y436				N437	N479
I489		G488				T486	T486	T486			Y484	Y484				K439	D480
						T487					T487	T486				D480	
						G488					Y491	T487					
						Q492											

CDR L1	CDR L2				FR L3									CDR L3		
N164	D182	S184	T185	R186	S195	G196	S197	G198	S199	D202	F203	T204	T206	S208	R223	S224	W226
Y436	Y440	Y442	Y442	Y475	L472	C474	P469	W436	W476	P470	P470	P470	L472	L472	Y436	Y436	S432
D480	Y442	Y475	N479		N473	Y475	P470	P469				A471			D480	Y484	T433
	N479				Y475		A471	P470							Y481		Y484
	D480						C474	C474							G482		
							Y475								Y484		

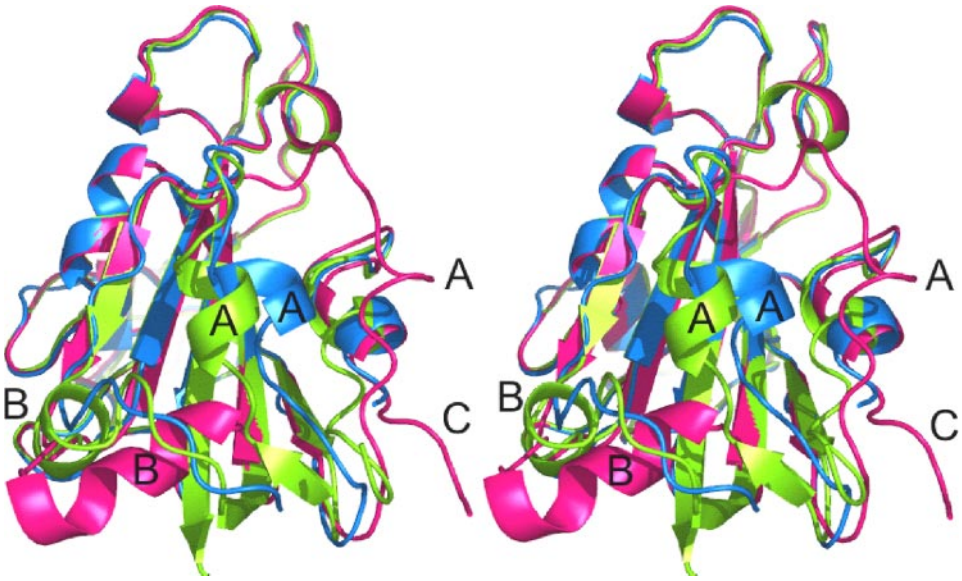

FIGURE 5. **Stereo comparison of the S1-RBD domain.** Uncomplexed (dimeric) S1-RBD is in *red*, complex with 80R antibody is in *green*; complex with ACE2 is in *blue*. Helical elements A and B and the C terminus are labeled. The receptor-binding surface, including the extended loop, is highly conserved in all three structures, lies at the back of the field, and is not visible in this view. Root mean square deviation values for pairwise comparisons are 0.9–1.1 Å for main chain residues excluding helix A (residues 350–360), helix B (370–381), and N and C termini before residue 323 or after residue 502. The small differences in these regions of the complexed S1-RBDs presumably arise from the different crystal environments. The large changes in the uncomplexed S1-RBD are a consequence of dimer formation.

The structure provides a rationale for previous mutagenesis studies. Thus, residue Asn^{479} is involved in both interfaces, and accordingly, mutations decrease both 80R binding and ACE2 binding (2–10-fold (7, 22)). Two further mutational sites that reduce antibody binding, at Asp^{454} and Glu^{452}, are not directly involved in the interface; their effect can be explained by the participation of these acidic residues in a salt bridge network that anchors the receptor/antibody binding interface to the S1 RBD core and the extended loop that wraps around the framework hairpin (Fig. 4*c*). One key difference between the two interfaces lies in the role of S1 residue Asp^{480}; thus, D480A or D480G mutations completely abolish binding to 80R but have no effect on ACE2 binding (7). Consistently, Asp^{480} lies at the heart of the S1-80R interface, making an intermolecular salt bridge to Arg^{162} (see supplemental Fig. 1) and an H-bond to Asn^{164} of 80R, whereasAsp^{480} makes no contacts in the S1-ACE2 complex. Binding of S1 RBD to either ACE2 or 80R is independent of glycosylation (6, 24); accordingly, all three potentially glycosylated asparagines (Asn^{318}, Asn^{330}, and Asn^{357}) in the S1 RBD are remote from the binding interfaces.

Structure of the Uncomplexed S1-RBD—We also determined the crystal structure of the uncomplexed S1-RBD (residues 318–510) at 2.2 Å resolution (Figs. 5 and 6 and Table 1). Compared with its structure in complex with either 80R or ACE2, the receptor-binding surface, including the extended loop, is essentially identical to its structure in the complexes. However, there are extensive rearrangements and increased ordering of the region distal to the 80R/ACE2-binding surface (Fig. 5), which lead to the formation of an extensive dimer interface with a buried surface area of ~2200 $Å^2$ (Fig. 6). The major reorganization occurs in three structural elements (secondary structure nomenclature as in Ref. 5) as follows: (i) the loop between strands 2 and 3 containing helix B reorganizes such that the new helix B is one turn longer and lies orthogonal to its position in the complexed structures; (ii) helix B from the neighboring monomer packs tightly across the dimer interface, causing helix A to shift by 10–12 Å to a new position adjacent to the C terminus; and (iii) the C terminus also undergoes a small concerted shift (~4 Å). The dimer is formed by the pairing of the β-sheets (via their β2-strands) and B-helices from each monomer and is largely hydrophobic in nature.

This dimer is predicted by the DCOMPLEX server to be physiologically relevant and to have a binding energy comparable with the S1-80R and S1-ACE2 binary complexes. In agreement with the structural data, gel filtration studies of S1 RBD indicate a monomer-dimer equilibrium in solution at micromolar concentrations (data not shown). Of note, it has been reported that the murine hepatitis coronavirus S1 domain also exists as a stable dimer (25).

The C termini of S1 RBD lie on the "lower" surface of the dimers (Fig. 6*a*), topologically consistent with their connection to the membrane-spanning S2 domain. At the lower surface of the dimer interface, two cysteine residues, from apposing B-helices (Cys^{378}), come into close proximity (Sγ–Sγ distance = 3.2 Å) but do not form a disulfide bond. We propose a model in which the S1 dimers present two preformed receptor-binding motifs pointing outward from the viral membrane surface. A plausible role for the S1 dimers is to cross-link S protein trimers (which trimerize via their S2 domains) on the viral surface (26), thus contributing to the structural integrity of the virion. Modeling two ACE2 receptors onto the S1 dimer leads to steric clashes between the receptors (Fig. 6*c*), which could explain why S1 is monomeric in crystals of the S1-ACE2 complex. Interestingly, in the S1-80R complex, S1 dimers still form, and in this case the two Cys^{378} residues remain in close apposition. However, the monomers are twisted with respect to their positions in the uncomplexed S1 dimers, and the hydrophobic interface is largely disrupted. *In silico* modeling of two 80R fragments onto the uncomplexed S1 dimer does not lead to steric clashes, and in this case the dimer rearrangement is presumably driven by competing lattice forces.

These observations raise the intriguing hypothesis that binding of multiple receptors *in vivo* promotes disruption of S protein dimers, perhaps in a redox-dependent fashion, thus priming S for subsequent membrane fusion events mediated by the S2 domains. A role for receptor-promoted viral uncoating is well established in the (nonenveloped) picornaviruses (27), and has also been described for the Env protein of avian leukosis

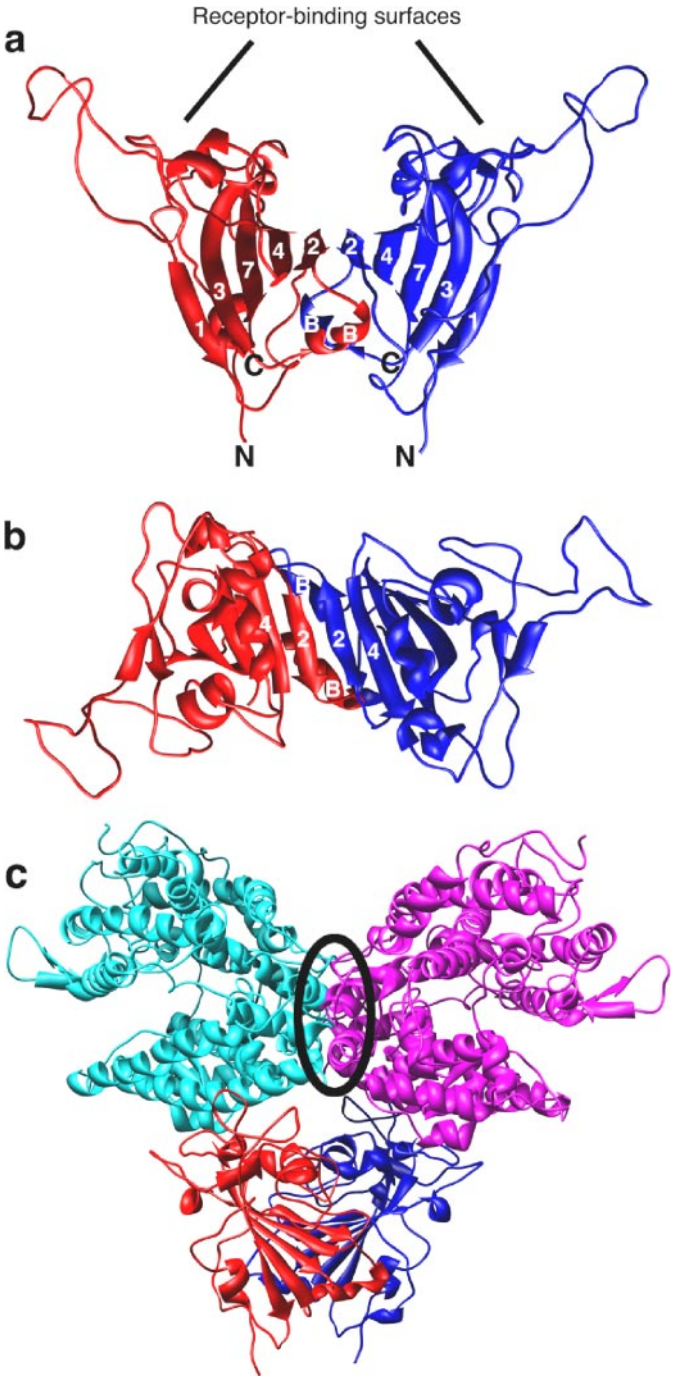

FIGURE 6. **Structure of the S1-RBD dimer.** *a*, S1 monomers are in *red* and *blue*, related by a vertical 2-fold axis. The receptor binding surfaces and C termini are indicated. *b*, same as in *a* but rotated by 90° about a horizontal axis to show the molecular dyad. *c*, hypothetical model of the S1-RBD dimer with two molecules of ACE2 bound, showing steric overlap (*circled*). The view is rotated about a vertical axis compared with *a* in order to minimize the overlap in projection. Two Fab fragments can bind the dimer without steric hindrance (not shown). A full-length dimeric antibody could presumably cross-link neighboring dimers on the viral surface, but the geometry is inappropriate for binding both sites on a single dimer simultaneously.

virus (28). Clearly, further experiments are required to explore this hypothesis.

Prospects for Immune Therapy—Marasco and co-workers (22) previously demonstrated that 80R IgG can neutralize all SARS-CoVs and SARS-like CoVs that evolved during the 2002–2003 outbreak. Because the 80R epitope on S1 overlaps so closely with the ACE2-binding site, we suggest that, for most residues on S1 at the binding site, antigenic drift on S that makes 80R ineffective is likely to abolish binding to ACE2 as well. A notable exception is the D480G mutation, which was found in the SARS-like CoVs from civet cats during the 2003–2004 winter season. These CoVs were likely responsible for an independent interspecies transmission that resulted in the infection of four patients in a mini 2003–2004 outbreak (23). The 80R antibody does not bind these mutants, as noted above; however, these viruses were also less pathogenic, and no cases of human-to-human transmission were reported.

By establishing the susceptibility and resistance profiles of newly emerging SARS-CoVs through early S1 genotyping of the neutralizing epitope of 80R, which we have now mapped in atomic detail, an effective immunotherapeutic strategy with 80R should be possible in a future SARS outbreak. In this setting, administration of 80R IgG would provide immediate protection for individuals; subsequently, the innate immune response would take effect, resulting in reduced virus titers and "superspreader" events, crucial for effective containment of the disease.

Acknowledgments—We thank V. Stojanoff and J. Jakoncic at beamline X6A, H. Robinson and G. Shea-McCarthy at beamline X29A (National Synchrotron Light Source), and K. Frankel at beamlines 12.3.1 and C. Trame at 5.0.3 (Advanced Light Source) for help with data collection, and C. Bakolitsa and L. Bankston for helpful discussion.

REFERENCES

1. Donnelly, C. A., Ghani, A. C., Leung, G. M., Hedley, A. J., Fraser, C., Riley, S., Abu-Raddad, L. J., Ho, L. M., Thach, T. Q., Chau, P., Chan, K. P., Lam, T. H., Tse, L. Y., Tsang, T., Liu, S. H., Kong, J. H., Lau, E. M., Ferguson, N. M., and Anderson, R. M. (2003) *Lancet* **361,** 1761–1766
2. Holmes, K. V. (2003) *J. Clin. Investig.* **111,** 1605–1609
3. Xu, Y., Lou, Z., Liu, Y., Pang, H., Tien, P., Gao, G. F., and Rao, Z. (2004) *J. Biol. Chem.* **279,** 49414–49419
4. Li, W., Moore, M. J., Vasilieva, N., Sui, J., Wong, S. K., Berne, M. A., Somasundaran, M., Sullivan, J. L., Luzuriaga, K., Greenough, T. C., Choe, H., and Farzan, M. (2003) *Nature* **426,** 450–454
5. Li, F., Li, W., Farzan, M., and Harrison, S. C. (2005) *Science* **309,** 1864–1868
6. Sui, J., Li, W., Murakami, A., Tamin, A., Matthews, L. J., Wong, S. K., Moore, M. J., Tallarico, A. S., Olurinde, M., Choe, H., Anderson, L. J., Bellini, W. J., Farzan, M., and Marasco, W. A. (2004) *Proc. Natl. Acad. Sci. U. S. A.* **101,** 2536–2541
7. Sui, J., Li, W., Roberts, A., Matthews, L. J., Murakami, A., Vogel, L., Wong, S. K., Subbarao, K., Farzan, M., and Marasco, W. A. (2005) *J. Virol.* **79,** 5900–5906
8. Otwinowski, Z., and Minor, W. (1997) *Methods Enzymol.* **276,** 307–326
9. Bragg, W. L., and Howells, E. R. (1954) *Acta Crystallogr.* **7,** 409–411
10. Wang, J., Kamtekar, S., Berman, A. J., and Steitz, T. A. (2005) *Acta Crystallogr. Sect. D. Biol. Crystallogr.* **61,** 67–74
11. Schwarzenbacher, R., Godzik, A., Grzechnik, S. K., and Jaroszewski, L. (2004) *Acta Crystallogr. Sect. D. Biol. Crystallogr.* **60,** 1229–1236
12. Vagin, A., and Teplyakov, A. (1997) *J. Appl. Crystallogr.* **30,** 1022–1025
13. McCoy, A. J., Grosse-Kunstleve, R. W., Storoni, L. C., and Read, R. J. (2005) *Acta Crystallogr. Sect. D. Biol. Crystallogr.* **61,** 458–464
14. Murshudov, G. N., Vagin, A. A., and Dodson, E. J. (1997) *Acta Crystallogr. Sect. D. Biol. Crystallogr.* **53,** 240–255

15. Brünger, A. T., Adams, P. D., Clore, G. M., DeLano, W. L., Gros, P., Grosse-Kunstleve, R. W., Jiang, J. S., Kuszewski, J., Nilges, M., Pannu, N. S., Read, R. J., Rice, L. M., Simonson, T., and Warren, G. L. (1998) *Acta Crystallogr. Sect. D. Biol. Crystallogr.* **54,** 905–921
16. Jones, T. A., Zou, J.-Y., Cowan, S. W., and Kjelgaard, M. (1991) *Acta Crystallogr. Sect. A* **47**, 110–119
17. Emsley, P., and Cowtan, K. (2004) *Acta Crystallogr. Sect. D. Biol. Crystallogr.* **60,** 2126–2132
18. Laskowski, R. J., MacArthur, N. W., Moss, D. S., and Thornton, J. M. (1993) *J. Appl. Crystallogr.* **26,** 283–290
19. Chothia, C., Lesk, A. M., Gherardi, E., Tomlinson, I. M., Walter, G., Marks, J. D., Llewelyn, M. B., and Winter, G. (1992) *J. Mol. Biol.* **227,** 799–817
20. Chothia, C., Lesk, A. M., Tramontano, A., Levitt, M., Smith-Gill, S. J., Air, G., Sheriff, S., Padlan, E. A., Davies, D., Tulip, W. R., and Colman, P. M. (1989) *Nature* **342,** 877–883
21. Jones, S., and Thornton, J. M. (1996) *Proc. Natl. Acad. Sci. U. S. A.* **93,** 13–20
22. Li, W., Zhang, C., Sui, J., Kuhn, J. H., Moore, M. J., Luo, S., Wong, S. K., Huang, I. C., Xu, K., Vasilieva, N., Murakami, A., He, Y., Marasco, W. A., Guan, Y., Choe, H., and Farzan, M. (2005) *EMBO J.* **24,** 1634–1643
23. Song, H. D., Tu, C. C., Zhang, G. W., Wang, S. Y., Zheng, K., Lei, L. C., Chen, Q. X., Gao, Y. W., Zhou, H. Q., Xiang, H., Zheng, H. J., Chern, S. W., Cheng, F., Pan, C. M., Xuan, H., Chen, S. J., Luo, H. M., Zhou, D. H., Liu, Y. F., He, J. F., Qin, P. Z., Li, L. H., Ren, Y. Q., Liang, W. J., Yu, Y. D., Anderson, L., Wang, M., Xu, R. H., Wu, X. W., Zheng, H. Y., Chen, J. D., Liang, G., Gao, Y., Liao, M., Fang, L., Jiang, L. Y., Li, H., Chen, F., Di, B., He, L. J., Lin, J. Y., Tong, S., Kong, X., Du, L., Hao, P., Tang, H., Bernini, A., Yu, X. J., Spiga, O., Guo, Z. M., Pan, H. Y., He, W. Z., Manuguerra, J. C., Fontanet, A., Danchin, A., Niccolai, N., Li, Y. X., Wu, C. I., and Zhao, G. P. (2005) *Proc. Natl. Acad. Sci. U. S. A.* **102,** 2430–2435
24. Chakraborti, S., Prabakaran, P., Xiao, X., and Dimitrov, D. S. (2005) *Virol. J.* **2,** 73
25. Lewicki, D. N., and Gallagher, T. M. (2002) *J. Biol. Chem.* **277,** 19727–19734
26. Lin, Y., Yan, X., Cao, W., Wang, C., Feng, J., Duan, J., and Xie, S. (2004) *Antivir. Ther.* **9,** 287–289
27. Nurani, G., Lindqvist, B., and Casasnovas, J. M. (2003) *J. Virol.* **77,** 11985–11991
28. Mothes, W., Boerger, A. L., Narayan, S., Cunningham, J. M., and Young, J. A. (2000) *Cell* **103,** 679–689